Neural Networks Are Tuned Near Criticality During a Cognitive Task and Distanced from Criticality In a Psychopharmacological Model of Alzheimer's Disease

Forough Habibollahi[1,3*], **Dechuan Sun**[2,3,*], **Anthony N. Burkitt**[1,5], **Chris French**[3,4]

[1] Department of Biomedical Engineering, The University of Melbourne, Parkville, VIC, Australia
[2] Department of Electrical and Electronic Engineering, The University of Melbourne, Parkville, VIC, Australia
[3] Neural Dynamics Laboratory, Department of Medicine, The University of Melbourne, Parkville, VIC, Australia
[4] Neurology Department, Royal Melbourne Hospital, Parkville, VIC, Australia
[5] Graeme Clark Institute for Biomedical Engineering, The University of Melbourne, Parkville, VIC, Australia

Abstract

Dynamical systems that exhibit transitions between ordered and disordered states are described as "critical" when the system is at the borderline between these states. The ability of criticality to explain a variety of brain properties, including optimal information processing, makes it of considerable interest to investigate whether these *in vivo* networks display critical behaviour, and whether some forms of cognitive impairment such as dementia might display altered critical behaviour. To investigate these questions, the activity of several hundred hippocampal CA1 neurons in freely-behaving mice was studied with miniscope widefield calcium imaging during rest, a novel object recognition task, and novel object recognition after administration of the amnesic drug scopolamine which acts as a psychopharmacological model of Alzheimer's disease. Utilizing rigorous metrics of criticality including the Deviation from Criticality Coefficient and Branching Ratio, the ensemble neural activity in the hippocampus was observed to display evidence of near-critical behaviour during rest periods, but moved significantly closer to a critical state when engaged in a cognitive task. The dynamics were observed to move significantly away from criticality during the cognitive task after scopolamine administration. In contrast to previous theoretical predictions, our results indicate that hippocampus neural networks move closer to criticality under cognitive load, and that critical dynamical regimes produce a near-optimal state for cognitive operations.

Keywords Criticality · Miniscope · Novel Object Recognition · Calcium Imaging · Cognitive Task · Alzheimer's Disease Model

1 Introduction

Recent investigations have revealed potential biomarkers of cognition and novel measures of information processing capabilities in neural activity of human and rodent subjects (Klyucherev et al., 2022; Wicklund and Petersen, 2013; Chen et al., 2022; Peterson et al., 2019; Cocchi et al., 2017). Criticality and brain state transitions to sub- or super-critical states have provided intriguing and novel perspectives into the neural mechanisms underlying cognitive functions. Increasing evidence suggests that localized episodes of bursting brain activity, analogous to avalanches in a sand pile, indicate that cognitive brain states are near criticality (Sreekumar et al., 2014, 2017; Nielson et al., 2015; Linkenkaer-Hansen et al.,

*Equal Contribution.

2001; Ma et al., 2019). A critical system is one that lies in a very narrow range between order and disorder. This means the brain's dynamical system, consisting of neurons as its information storage and processing units, is capable of phase transitions. In a near-critical condition, there are long-range connections present between units that produce ordered structures accompanied by some level of disordered fluctuations in the system. This is in contrast with a sub-critical system where we observe spatial structure with low fluctuation capacity and also with a super-critical system where high frequency fluctuations are present with low levels of spatial correlation. Near-critical dynamics gives rise to an increased dynamic range (Deco and Jirsa, 2012; Deco et al., 2011), which is equivalent to having an elevated number of *cognitive sets* or stored memories (Scarpetta and de Candia, 2013). Complementary studies in this field support these findings, indicating that criticality optimizes information capacity and processing capabilities of neural activity (Fagerholm et al., 2016; Shew et al., 2011; Boedecker et al., 2012).

There is a growing body of experimental evidence that cortical networks exhibit *neuronal avalanches* (cascades of propagating activity governed by power-laws), from *in vivo* studies from the hippocampus and neocortex in rats and primates (Nádasdy et al., 1999; Hoffman and Mcnaughton, 2002), premotor and motor cortex of awake monkeys (Petermann et al., 2009), the developing cortex of the anesthetized rat (Gireesh and Plenz, 2008), and the whole-brain dynamics of zebrafish (Ponce-Alvarez et al., 2018). These studies have demonstrated that spontaneous activity in each of these networks is capable of producing highly repeatable spatial-temporal patterns indicating the existence of neuronal avalanches. Evidence of neuronal avalanches have also been found *in vitro* in local field potentials (LFPs) of spontaneous activity in acute cortex slices (Stewart and Plenz, 2006; Beggs and Plenz, 2003), slice cultures (Beggs and Plenz, 2003), cultured hippocampal neurons (Pu et al., 2013), and cultured human stem cells (Heiney et al., 2019). Similarly, criticality has been linked to stimulus detection in *ex vivo* models of cortical activity (Clawson et al., 2017).

Increasing evidence identifies a link between critical dynamics in the brain and cognitive behaviour (Sreekumar et al., 2014, 2017; Nielson et al., 2015). The recognition of this relationship originates from the long-range temporal correlations observed in human activity and memory, which scale across many orders of magnitude (Bhattacharya et al., 2005; Palva et al., 2013).

Additionally, a number of previous studies on healthy adults during working memory and cognitive tasks have reported power-law scaling of response time fluctuations (Altamura et al., 2012; Simola et al., 2017). Subsequently, however, the implications of these results for criticality was called into question, as power-law scaling was found to have a possible explanation arising from random noise (Touboul and Destexhe, 2017).

Consequently, experimental evidence is still required to shed light on how criticality is related to the brain's response to increasing cognitive loads. Can increased cognitive load shift random behavior toward scale-free behavior near a critical point? Whether criticality is the default resting state of cortical networks and the extent to which it is present during cognition and perception-related tasks during learning remains a key question that is addressed here. Identifying a transition from sub-critical states to near-criticality during the emergence of a learned behaviour can potentially assist in answering this question.

In this study we used wide-field calcium imaging of the hippocampal CA1 region in order to undertake a more detailed analysis of the dynamics of the neuronal activity in the hippocampus. To monitor the activity of neural ensembles during cognitive tasks, *in vivo* calcium imaging was performed on the hippocampal CA1 region of freely moving mice. This was accomplished using a miniaturized microscope (Ghosh et al., 2011; Aharoni et al., 2019), which made it possible to record the activity of a large group of neurons simultaneously by measuring calcium levels. The hypothesis investigated in this study is that hippocampal neural networks move closer to criticality with an increased cognitive load during a task, chosen here to be Novel Object Recognition (NOR), when compared to the resting state. In this task, an animal is initially presented with two identical objects, followed by a delay period, and then one of the familiar objects is replaced with a novel object which is similar but not identical to the familiar objects. The time spent exploring each object is recorded, and the ability of the animal to recognize the novel object is assessed by comparing the exploratory behavior towards the novel object with that towards the familiar one. Our findings suggest that switching from inactivity to a cognitively active state modulates the network's distance from criticality. Moreover, we demonstrate that administration of scopolamine as a non-specific antagonist of mAChRs (Hulme et al., 1978; Lee and El-Fakahany, 1985), which greatly impairs spatial memory encoding (see (Hayward, 2004) and (Klinkenberg and Blokland, 2010) for a review), and hence animal performance in the NOR test, drives the dynamics of the neuronal system further from the critical point. Our findings imply that being tuned near criticality is potentially the near-optimal state for the brain network while engaged in a cognitive task, given that at criticality, the dynamical range, and the information content and transmission are maximized.

2 Results

To examine whether critical dynamics arise in CA1 networks in freely behaving mice during a cognition-related task, we recorded from 8 healthy animals while moving freely in their home cage as well as both familiarization and testing phases of the NOR test (see Supplementary Materials). The animals were subject to GCaMP6f viral infusion followed by GRadient INdex (GRIN) lens implantation. After recovering from the surgeries, a metal baseplate used to support the miniscope device was attached to the animals' heads which were then connected to the data acquisition software via a coaxial cable during recording sessions. We recorded from populations of 290 ± 42 CA1 neurons in 15-minute recording sessions. The calcium events associated with the detected neurons were derived from the recordings and used to identify neuronal avalanches from the population activity. Neuronal avalanches were defined to start and stop when the population activity (i.e., total number of contributing events) surpassed a certain threshold of the entire network activity. These avalanches were then employed to identify the criteria for criticality. Firstly, scale-free dynamics in both temporal and spatial domains and power-law distributions of observing avalanches with a certain size (S) (number of contributing events) and duration (D) (time) are the hallmark of criticality. Second, in critical systems, the power-law exponents fit to avalanche size (τ) and duration (α) are related by a third predicted exponent as $\beta_{\text{pred}} = \frac{\alpha-1}{\tau-1}$. Employing the exponent relation between S and D near-criticality, $\langle S \rangle = D^{\beta_{\text{fit}}}$, the mean avalanche size ($\langle S \rangle$) observed at a given duration can be predicted using α and τ. Now when $\langle S \rangle$ is plotted against avalanche duration, the difference

between the empirically derived β_{fit} and the predicted β_{pred} is called the Deviation from Criticality Coefficient (DCC) as the second and strongest indicator of criticality which is minimized near the critical state. Branching Ratio (BR) is the third measure and demonstrates the ratio between the number of active units at time $t + 1$ to the number of active units at time t which is tuned near 1 at criticality. The Shape Collapse error (SC error) is the final metric of criticality to demonstrate how accurately avalanches of all profiles can be collapsed to the same universal shape. The error in finding this universal scaling function is minimized in criticality (see Supplementary Materials, (Ma et al., 2019; Wilting and Priesemann, 2018; Spitzner et al., 2021; Marshall et al., 2016) for details). These measures enable us to evaluate whether a task involving the recognition memory moves the network dynamics closer to criticality compared to rest state spontaneous activity recorded in the home cage.

2.1 Hippocampus neuronal networks are tuned near-criticality during a cognitive task

We compared the criteria for criticality derived from recording sessions when the animals were in the testing phase of the NOR experiments and when they were freely exploring their home cage (see Supplementary Materials). The NOR experiment evaluates the recognition memory of the animals and particularly involves their spatial memory performance. Hence, it applies an increased cognitive load to the neuronal network while the animals are exploring both novel and familiar objects actively utilizing their spatial memory. We found that when mice were retrieving the representation of the familiar object from their memory helping them to successfully distinguish between the novel and the familiar object, the network of neurons was closer to a critical state compared to the dynamics of this network during rest state recording in the home cage.

We used 8 healthy adult male C57BL/6 mice in recording sessions of 15 minutes in their home cage as well as both phases of the NOR test. Figure 1.a shows an animal being recorded by a miniscope in its home cage. These animals are then exposed to the experimental arena for habituation (see Supplementary Materials) before the familiarization phase (two similar objects) and the testing phase (one familiar and one novel object) of the NOR experiment. Figure 1.b is an image captured from the experimental setting in both phases of NOR. The animal trails during these phases as well as the object locations in the arena are recorded and drawn by the top-view-based behavior analysis system used in this work (TopScan: TopView Analyzing System 2.0; Clever Sys Inc). A sample trail shown in Figure 1.c outlines the higher amount of exploration time around the novel (red) object in the testing phase. The behavioural results from all 8 animals showed that on average, these healthy mice spend a higher amount of time exploring the novel object in the testing phase while no significant difference is detected between the exploration times of the two similar objects in the familiarization phase (see Figure 1.d).

The miniscope recordings were processed and using the Constrained Non-negative Matrix Factorization (CNMF) algorithm (Zhou et al., 2018; Pnevmatikakis et al., 2016; Kotliar et al., 2019) the spatial footprints of the detected neurons as well as the corresponding calcium events are extracted (see Supplementary Materials for more details). Using these calcium events, the activity of each neuron in each recorded frame (i.e., 33.3 ms) was binarized, based on being active or not, i.e., 1 or 0. The neuronal avalanches were calculated as cascades of events that started and

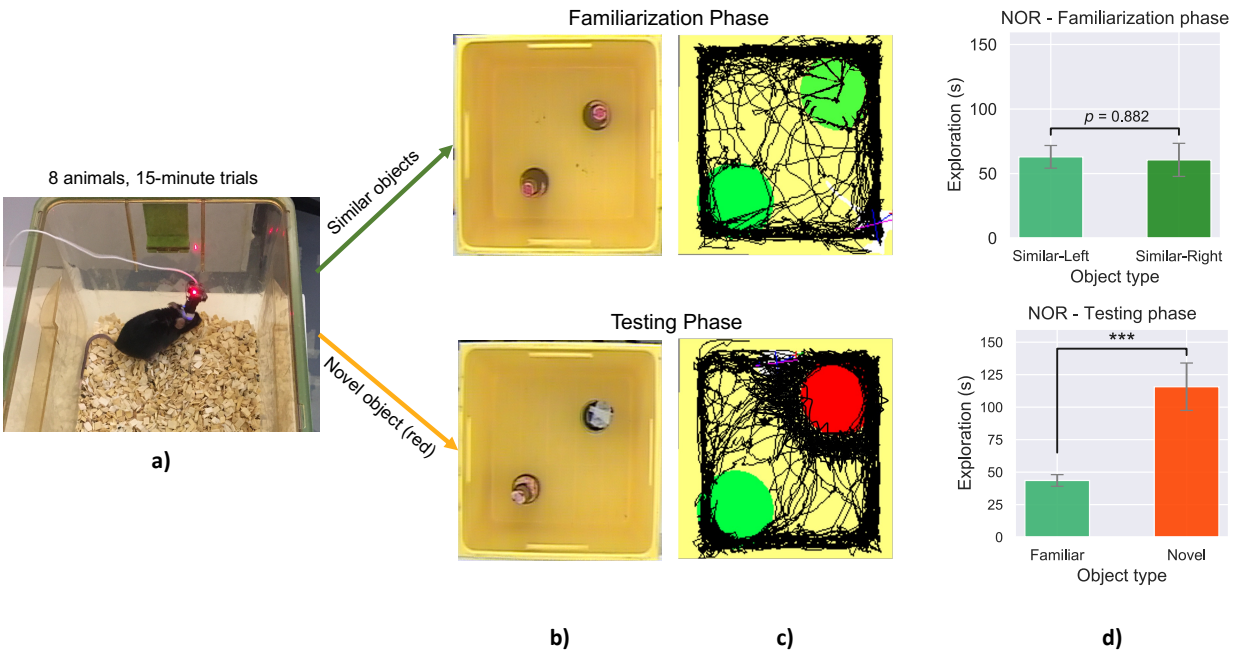

Figure 1: NOR experimental setup and behavioural performance of the mice. a) A mouse with the miniscope device mounted on its head being recorded in its home cage. **b)** The setting of both phases in the NOR experiment; top: familiarization phase with 2 similar objects inside the arena, bottom: the testing phase where one of the familiar objects is replaced with a novel one. **c)** Sample mouse trails in black recorded using the TopScan software in the top: familiarization and bottom: testing phase of the NOR experiment. The novel object in the testing phase is colored red. **d)** The average exploration time around each of the objects in the top: familiarization and bottom: testing phase. In the familiarization phase, there was no significant difference detected between the average time spent exploring each of the objects. However, the exploration time of the novel object in the testing phase was significantly higher than the familiar object (One-way ANOVA test, *** $p-$value < 0.005). Error bars, SEM.

stopped when passing a certain threshold of network activity (i.e., the total amount of activity captured in the frame). The results were robust to changes of this threshold in a range of 30 to 70 % of network activity. These avalanches were then utilized in extracting the criticality metrics. Figure 2.a-b show comparisons of the power-law distributions and the DCC measures obtained from one of the animals in its home cage and the testing phase of the NOR experiment. While power-law distributions could be fit to the avalanche size and duration in both groups of recordings ($\alpha = 1.937 \pm 0.070$, $\tau = 2.597 \pm 0.091$ in NOR experiments (testing phase); and $\alpha = 1.540 \pm 0.056$, $\tau = 2.367 \pm 0.100$ during cage recordings), the lower DCC measure in Figure 2.b indicates a system operating closer to criticality. Figures 2.c-e illustrate the distribution of the criticality metrics in different recording sessions in the cage or the testing phase of NOR (NOR: indicates the testing phase of the experiment in the figures of this article). Comparison of the NOR (colored in cyan) and Cage (colored in orange) sessions indicates the shift of the CA1 network dynamics towards criticality during the task-present sessions and the testing phase of NOR.

2.2 Scopolamine-induced memory impairment drives system dynamics away from criticality

Previous studies have shown that the neurotransmitter acetylcholine plays a significant role in the process of acquiring and encoding new information (Hasselmo, 2006). Additionally, it has been observed that the administration of acetylcholine muscarinic receptor antagonists, such as scopolamine, can significantly impair recognition memory

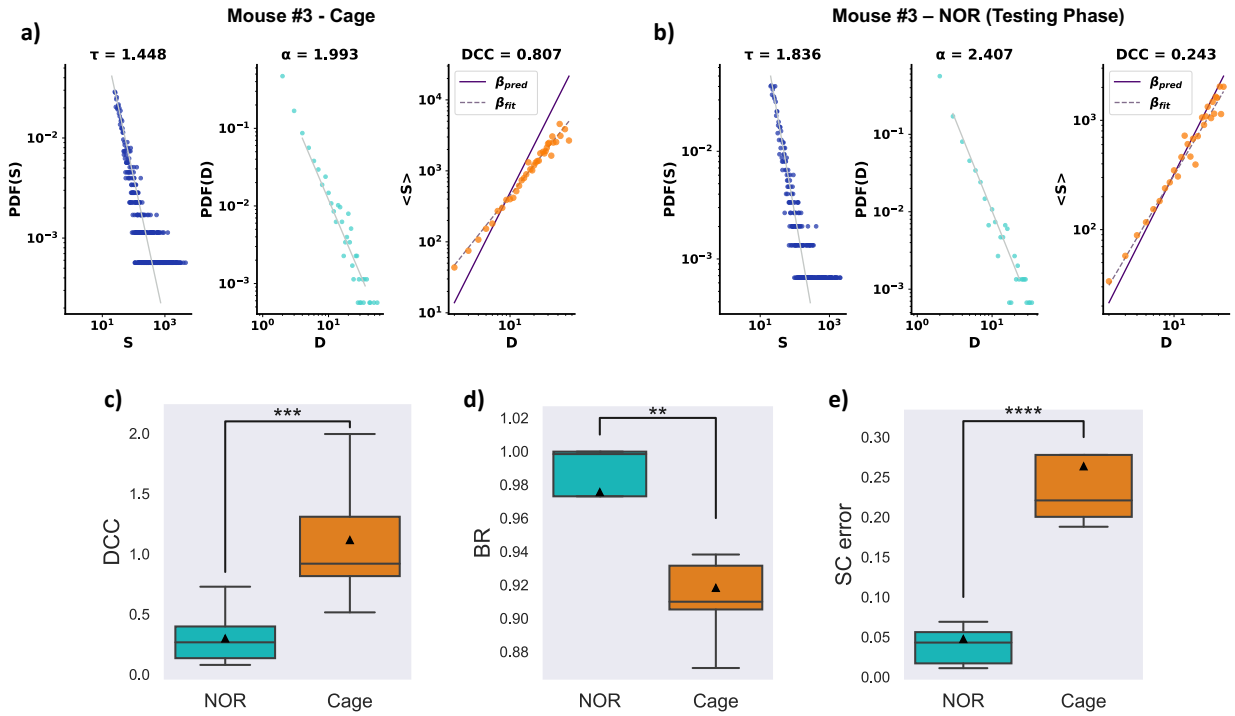

Figure 2: Criticality arises as the animals are engaged in a cognitively demanding task, NOR. Avalanche are quantified as a function of the number of contributing calcium events (S) from all neurons in the region of interest and the duration of the avalanche (D). The Probability Distribution Function (PDF) for detecting avalanches of a specific size (blue) or duration (cyan) can be fit with power-laws, resulting in the generation of two exponents (τ, α) respectively; in the log-log plot, the exponent represents the slope of the line. In critical systems, the following relation holds between the size and duration exponents: $\beta_{\text{pred}} = \frac{\alpha-1}{\tau-1}$. Deviation from criticality as measured by the Deviation from Criticality Coefficient (DCC), is the quantitative difference between the predicted β_{pred} exponent (solid purple line) and the observed β_{fit} exponent (dashed gray line). **a)** The PDF fitted to avalanche size and duration and the DCC measure in the recordings from Mouse number 3 inside the home cage. **b)** The PDF fitted to avalanche size and duration and the DCC measure in the recordings from Mouse number 3 during the testing phase of the NOR experiment. **c, d, e)** DCC, BR, and SC errors extracted for all the recordings and compared between Cage and the testing phase of the NOR experiment. The illustrated trend in all measures supports the conclusion that the system tunes near-criticality during a cognition task such as NOR. The NOR recordings display DCC and SC error values significantly closer to 0 and branching ratios significantly closer to 1; features that are missing in the cage recordings. (One-way ANOVA test, **** $p-$value < 0.0005, *** $p-$value < 0.005, ** $p-$value < 0.05).

(Creighton et al., 2019; Dodart et al., 1997; Tinsley et al., 2011; Kruk-Słomka et al., 2014; Kowalczyk et al., 2020). To further evaluate the potential roles of criticality-tuned dynamics in recognition memory, one month after the completion of NOR experiments, the animals were employed in another set of NOR experiments. At this stage, 2 mice were removed from the study due to showing signs of reduced mobility and a significant increase in the level of their struggle while mounting miniscope devices. In the first week, the animals were recorded after injection of saline (0.9% NaCl, intraperitoneal, i.p.; 10 mL/kg body mass), 20 minutes before the familiarization phase of NOR (Tinsley et al., 2011). After 2 weeks of no experiments, the same 6 animals were injected by a dose of scopolamine (intraperitoneal, i.p.; 0.6 mg/kg body mass) 20 minutes before the first phase of NOR. The performance of the animals was then compared among the two stages of the study to evaluate the effects of scopolamine-induced memory deficits on the criticality of the hippocampus CA1 network. The number of detected neurons from the recordings changed to 284 $\pm$ 14 in these experiments not representing any significant change compared to the pre-injection experiments (p = 0.936, One-way ANOVA test). The average firing rate of the population showed a non-significant reduction in the trials post

scopolamine administration compared to saline-injected control group (3.218 $\pm$ 0.839 Hz and 2.932 $\pm$ 0.712 Hz, saline and scopolamine administration respectively; p = 0.563, One-way ANOVA test).

First, to identify whether scopolamine impairs the performance of the animals in the NOR experiment, we measured the *discrimination index*, the *global habituation index*, *recognition index*, and the *preference index* (Antunes and Biala, 2012) to evaluate the object recognition memory during the NOR test. The discrimination Index (DI), allows discrimination between the two objects in the testing phase of the experiment. DI uses the difference in exploration time for the novel and familiar object, dividing it by the total amount of exploration of both objects. The score obtained from this test ranges from +1 to -1, where a positive score indicates that the subject spent more time with the novel object, a negative score indicates that the subject spent more time with the familiar object, and a score of zero indicates no preference. The global habituation index (GI) is calculated by dividing the total time spent exploring the two objects during the familiarization phase by the total time spent exploring them during the testing phase. GI tends to be lower than one in healthy animals. The Recognition Index (RI) is calculated as the time spent exploring the novel object divided by the total time spent exploring both objects during the testing phase, and is considered the primary measure of retention (Schindler et al., 2010; Gaskin et al., 2010; Botton et al., 2010). Therefore, an RI index above 0.5 indicates novel object preference, and below 0.5 shows familiar object preference. Finally, the preference index (PI) is calculated as the ratio of the time spent exploring one of the two objects during the familiarization phase to the total time spent exploring both objects. Therefore, a preference index above or below 0.5 indicates object preference, and a value close to 0.5 shows no preference.

The results in Figure 3 compare the NOR experiments following saline (3.a-b) and scopolamine 3.c-d) injections. While there is a significant difference between the exploration times of the familiar and novel object in the testing phase of saline experiments (3.b), this difference disappears by scopolamine injection (3.d). Additional evidence of scopolamine impairing the recognition memory of the mice were found using the introduced indices of DI, GI, RI, and PI, as represented in Figure 3.e. Compared to saline control group, scopolamine injection significantly reduced the ability to discriminate the novel object (DI), increased the ratio of the global exploration time in the familiarization phase to the testing phase (GI), decreased the time spent exploring the novel object relative to the total object investigation time in the testing phase (RI), and kept the preference index between any of the two similar objects in the familiarization phase near 0.5, similar to saline controls. All these results further validate previous findings that scopolamine administration causes spatial memory deficits affecting the mice recognition memory in the NOR experiments.

Consequently, we also found that the dynamics of the system is driven further from criticality in the testing phase of the NOR experiment when the mice's memory was impaired by scopolamine administration compared to saline controls (see Figure 4). The comparison of the three criticality metrics (i.e., DCC, BR, and SC error) was repeated for the NOR (Saline), NOR (Scopolamine), and Cage groups. The results support our hypothesis that the NOR (Saline) group has a significantly lower average DCC and SC Error while showing a significantly higher BR measure on average. The statistical significance of these findings was evaluated using a pairwise post hoc Tukey's test. The results are shown in Figure 4 indicating that in all three criticality metrics, there is a statistically significant difference between the Cage and

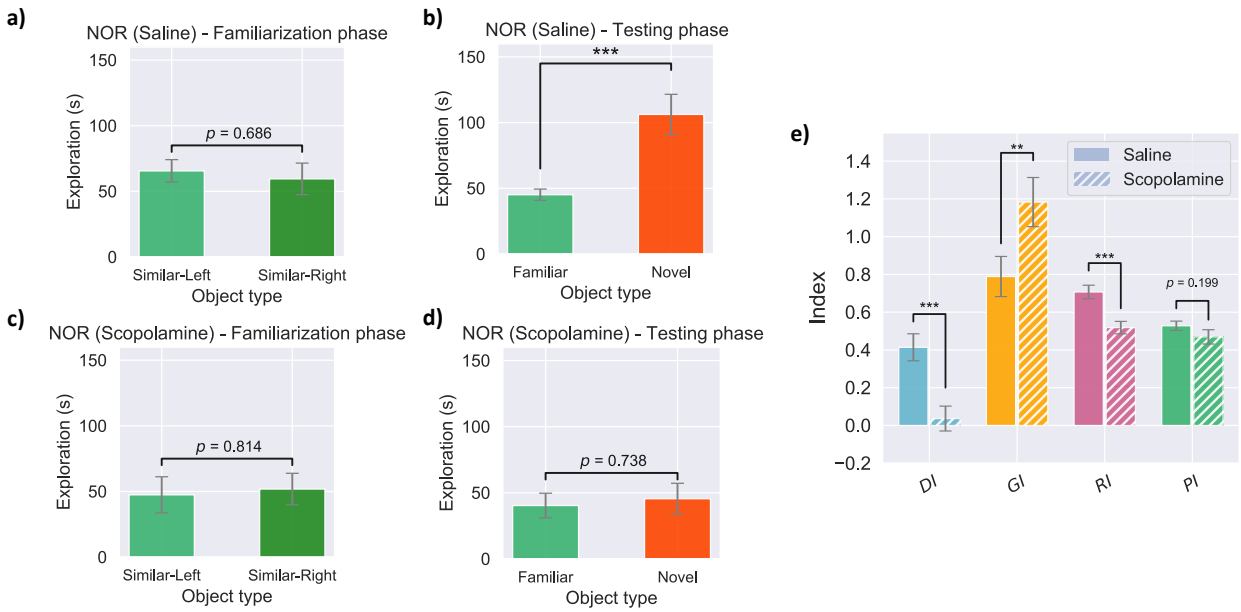

Figure 3: Scopolamine administration impairs spatial memory and disrupts the mice's performance in the NOR testing phase compared to saline-injected control experiments. a, b) Saline control NOR experiments. The average exploration time around each of the objects in the **a)** familiarization and **b)** testing phase. In the familiarization phase, there was no significant difference detected between the average time spent exploring each of the objects while in the testing phase a significantly higher average exploration time was detected around the novel object (One-way ANOVA, *** $p-$value < 0.005). **c, d)** Scopolamine injected NOR experiments. The average exploration time around each of the objects in the **c)** familiarization and **d)** testing phase. Scopolamine impairs spatial memory affecting the animals' performance in the NOR test. There was no significant difference observed between the average exploration time of the animals around the familiar and the novel object in the testing phase after scopolamine injection (One-way ANOVA test, $p-$value = 0.738). **e)** Comparing the DI, GI, RI, and PI indices in two groups of saline and scopolamine-injected animals. The significant decrease in the discrimination and recognition indices (One-way ANOVA, *** $p-$value < 0.005) as well as the significant increase in the global habituation index (One-way ANOVA, ** $p-$value < 0.05) after the scopolamine administration all indicate spatial and recognition memory deficits induced by scopolamine. Error bars, SEM.

NOR (Saline) groups (the orange and cyan bars respectively) with the NOR (Saline) group showing dynamics closer to criticality. This is while the Cage and the NOR (Scopolamine) groups (the orange and pink bars respectively) do not unveil a significant difference in any of the metrics. The NOR (Saline) and NOR (Scopolamine) groups also show dynamics that are significantly different in terms of all the three criticality metrics.

3 Discussion

There is increasing evidence that brain neuronal ensemble activity displays critical dynamics when performing cognitive activity (Sreekumar et al., 2014, 2017; Nielson et al., 2015). The results here from several hundred hippocampal CA1 neurons using a wide-field calcium imaging technique (miniscope), in 8 freely-behaving mice, for the first time shows that switching from inactivity to a cognitively active state moves the hippocampal network activity closer to criticality. This is manifested as a decrease in the Deviation from Criticality Coefficient (DCC) and Shape Collapse error (SC error), while increasing the Branching Ratio (BR). Although the spontaneous activity of hippocampal neurons in the rest state displayed dynamical properties of critical systems, with neuronal avalanches showing temporal and spatial power-law distributions, during the novel object recognition task the system moved significantly closer to a critical state.

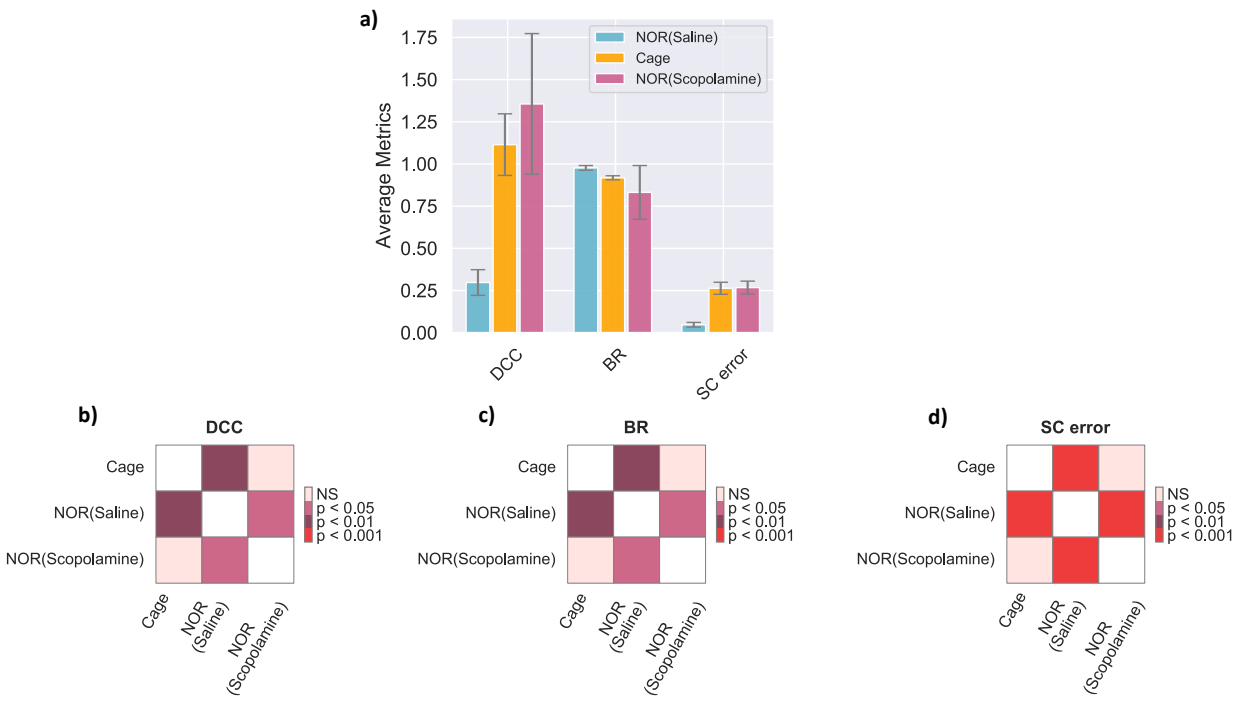

Figure 4: The recognition and spatial memory deficits induced by scopolamine injection tune the network away from criticality compared to saline controls showing dynamics more similar to rest periods in the home cage. a) Comparison of the average extracted metrics of criticality in the cage, the testing phase of NOR(Saline), and the testing phase of NOR(Scopolamine) experiments. In all three measurements, the NOR(Scopolamine) test indicates a system that is significantly closer to a critical state compared to both the cage and NOR(Saline) groups. Error bars, SEM. **b, c, d)** The significance matrix using pairwise post hoc Tukey's test. A significant difference is detected in all three metrics between cage and NOR(Saline) as well as NOR(Scopolamine) and NOR(Saline). There is no significant difference detected between cage and NOR(Scopolamine) groups in any of the measures indicating that both systems are tuned far from criticality.

Conversely, the network dynamics was observed to shift away from criticality when cognitive performance was impaired by the amnestic anticholinergic agent scopolamine. The results demonstrate that specifically during engagement in a cognitive task, hippocampus neural networks utilize the benefits of optimized transmission, dynamical range and information content associated with critical dynamics. This is in contrast to previous reports of critical or near-critical dynamics in the rest state (Cocchi et al., 2017; Beggs and Plenz, 2003; Werner, 2013; Ponce-Alvarez et al., 2018).

Multiple previous studies have investigated critical phenomena from both *in vitro* (Beggs and Plenz, 2003; Gireesh and Plenz, 2008; Tetzlaff et al., 2010; Habibollahi et al., 2022) and *in vivo* spike recordings (Hahn et al., 2017; Dahmen et al., 2019; Ma et al., 2019; Wilting and Priesemann, 2019), to even coarser-grained neural recording modalities (Ponce-Alvarez et al., 2018; Shew et al., 2015; Bellay et al., 2015), including electroencephalography (EEG) (Linkenkaer-Hansen et al., 2001; Jannesari et al., 2020), magnetoencephalography (MEG) (Toker et al., 2022; Palva et al., 2013; Fagerholm et al., 2015), and functional magnetic resonance imaging (fMRI) (Fraiman et al., 2009; Kitzbichler et al., 2009). A recent surge of interest has arisen from the development of large-scale multineuronal recording techniques (Dahmen et al., 2019; Fosque et al., 2021; Ponce-Alvarez et al., 2018; Fagerholm et al., 2021; Stringer et al., 2019) that allow greatly enhanced spatial and temporal resolution of ensemble dynamics. Earlier studies identified critical dynamics with power law observables of both event lifetime and spatial distributions. Evidence of

these power-law observables has been found in a wide range of experimental studies in *in vitro* (Beggs and Plenz, 2003; Gireesh and Plenz, 2008; Friedman et al., 2012; Tetzlaff et al., 2010) and *in vivo* (Tagliazucchi et al., 2012; Jannesari et al., 2020; Gautam et al., 2015; Clawson et al., 2017; Miller et al., 2019), using different recording methods (Priesemann et al., 2014; Bellay et al., 2015; Fagerholm et al., 2015; Lombardi et al., 2021). Nonetheless, it has become apparent that these measures are necessary but not sufficient to identify critical dynamics, since many noncritical processes also produce power laws (Priesemann and Shriki, 2018; Touboul and Destexhe, 2010). Consequently, several more rigorous metrics have been developed and recently implemented (Friedman et al., 2012; Sethna et al., 2001; Marshall et al., 2016; Ma et al., 2019; Wilting and Priesemann, 2018), three of which have been utilised in the current study.

Our study combines miniscope wide-field multineuronal recordings with analysis of several metrics that are considered to reliably characterize critical behaviour (Ma et al., 2019). With recordings from freely-behaving animals in the hippocampal CA1 region, an area well known to be associated with memory encoding and cognitive tasks, criticality metrics were measured in three different modes: rest (cage recordings), cognitive task (NOR-saline recordings), and a drug-affected state (NOR-scopolamine recordings) in which task performance is impaired. The miniscope technique in principle provides significant opportunities for critical dynamics observation – primarily it allows a large number of neurons comprising a substantial proportion of the activated network to be recorded over considerable periods of time, with naturalistic behaviours in freely moving animals. However calcium imaging does not achieve the same temporal resolution as electrophysiological recording, due to the slow dynamics of calcium activity and fluorophores. Nonetheless, we find this method is suitable for this study as it allows single action potentials to be detected at low frequencies, within the firing rates typically observed in cognitive tasks with electrode recordings (Power and Sah, 2002; Harding et al., 2020). Miniscopes in mouse hippocampus have been used extensively to record place cell behaviour (Sun et al., 2021; Sotskov et al., 2022; Wirtshafter and Disterhoft, 2022), phenomena generated by complex information encoding and decoding, with similar results to electrophysiological recording, suggesting a high level of functional correlation between miniscope and electrophysiological methods. Calcium signals from multiphoton imaging have been used as the basis for a brain computer interface, again demonstrating a close relationship between calcium transients and "ground truth" electrophysiological signals (Trautmann et al., 2021; Clancy et al., 2014).

Scopolamine treatment was used in the study because it has well-described effects on memory and has been considered as a model of neurodegenerative conditions such as Alzheimers disease, in which cholinergic neurotransmission to the hippocampus is known to be impaired (Beatty et al., 1986; Hasselmo and Wyble, 1997; Kowalczyk et al., 2020; San Tang, 2019; Bajo et al., 2015). We hypothesized that the cognitive degradation would be accompanied by a changes in criticality measures, reflecting the impaired functional state of the system. The results support this hypothesis, tending to support the notion that optimal cognitive performance is characterized by brain states closer to criticality. Scopolamine has been found in some studies to directly affect calcium conductances, raising the question whether the miniscope measurements might be affected (Power and Sah, 2002; Gähwiler and Brown, 1987; Tsubokawa and Ross, 1997). This is unlikely as other scoplolamine experiments in this laboratory (Sun et al., 2021) with miniscopes, as well

as electrophysiological studies (Brazhnik et al., 2003, 2004), have shown similar effects, making a defect in calcium signal quality unlikely. Consequently, it appears that the memory deficits caused by scopolamine administration are likely related to cholinergic functional impairment rather than a direct effect on the dynamics of the system, which in theory could reduce memory capacity. It will be of interest to see if future criticality measurements can be used as a biomarker of cognitive impairment in experimental models of neurodegenerative disease, which could also correlate and guide treatment strategies.

An interesting and contentious question related to the current study is whether brain dynamics are situated exactly at criticality or at a near-critical state. Some studies find dynamics situated precisely at the critical point (Beggs and Plenz, 2003; Bellay et al., 2015; Miller et al., 2019; Jannesari et al., 2020), while others, mostly from *in vivo* spiking studies, report brain dynamics are just intruding into the sub-critical region (Priesemann et al., 2014; Hahn et al., 2010; Ma et al., 2019; Wilting and Priesemann, 2019; Priesemann et al., 2013; Ribeiro et al., 2010) similar to our findings. The presence of a sub-critical brain state has some interesting implications. A near-critical state possesses computational properties similar to criticality, but with a slight reduction in other computational properties associated with the adjacent sub-critical phase. This is because the critical region is 'stretched' in finite and input-driven systems like the brain (Wilting and Priesemann, 2018). It therefore still optimizes information processing, but being at a certain distance from the critical point should reduce the incidence of dysfunctional neural behaviour, of which seizures are a possible manifestation (Priesemann et al., 2014). Nevertheless, another conceptual framework has been recently proposed, classifying brain dynamics as "quasicritical" (Williams-García et al., 2014; Beggs, 2022). This proposes that due to the consistently present external drive applied to all functional neuronal ensembles, the fully inactive phase for BR< 1 is no longer present, and thereby, we no longer observe a phase transition between active and inactive states. Due to the absence of this phase transition, there is also no longer a "critical" point. The presence of an external drive prevents cortex from reaching a critical phase transition point, and based on available data, it is expected that such a drive will always be present. Instead, this type of dynamics is referred to as "quasicritical". Whether the findings presented here are interpreted as slightly sub-critical or quasicritical, we found that there was a transition towards a critical regime with increased cognitive load. We suspect that this will be generally observed with increased cognitive loads, and it will be of interest to see if this is confirmed in a range of cognitive tasks.

With the assumption that optimal brain function will be associated with critical dynamical behaviour, a number of previous studies have attempted to equate a wide range of pathological states with suboptimal critical behaviour, including epilepsy, schizophrenia, major depressive disorders and Parkinson's disease - see (Zimmern, 2020) for a review. While some associations have been found, these reports are often substantially limited by inferring critical behaviour only from power law calculations of potentially relevant variables. The present study is useful in verifying that at the level of neural ensembles, at or close to real time neural processing speeds, these dynamics are observed during a cognitive task, and vary behaviourally and with scopolamine administration. The current observations place the hypotheses of these previous studies on a firmer foundation, and will be of great interest to replicate in animal models of these diseases. Hopefully, it will be possible to find ways to apply more rigorous criticality metrics in the

clinical setting in order to further explore possible relationships between classical neuropathology and systems-level dynamical dysfunction, leading to the development of improved biomarkers and potential therapies.

To conclude, if the necessity of a near-critical state is established for the successful transmission and storage of information in highly-demanding cognitive situations, our research, among other related studies, can pave the way toward future work in restoring the critical state of disrupted neuronal networks.

Acknowledgements

F.H. was supported by the Melbourne Research Scholarship. A.N.B. was supported by the Australian Government through the Australian Research Council's Discovery Projects funding scheme (Project DP220101166). C.F. was supported by the RMH Neuroscience Foundation.

Author contributions

Conceptualization, C.F., F.H, and A.N.B; Methodology, F.H.; Investigation, F.H., D.S., C.F. and A.N.B.; Writing – Original Draft, F.H.; Writing – Review & Editing, F.H., D.S., C.F. and A.N.B.; Funding Acquisition, C.F., and A.N.B.; Resources, C.F.; Supervision, C.F., and A.N.B

Declaration of interests

The authors declare no competing interests.

References

Daniel Aharoni, Baljit S Khakh, Alcino J Silva, and Peyman Golshani. All the light that we can see: a new era in miniaturized microscopy. *Nature Methods*, 16(1):11–13, 2019.

Mario Altamura, Brita Elvevåg, Gaetano Campi, Michela De Salvia, Daniele Marasco, Alessandro Ricci, and Antonello Bellomo. Toward scale-free like behavior under increasing cognitive load. *Complexity*, 18(1):38–43, 2012.

M Antunes and Grazyna Biala. The novel object recognition memory: Neurobiology, test procedure, and its modifications. *Cognitive Processing*, 13(2):93–110, 2012.

R Bajo, S Pusil, María Eugenia Lopez, L Canuet, Ernesto Pereda, Daria Osipova, F Maestú, and Eero Pekkonen. Scopolamine effects on functional brain connectivity: a pharmacological model of Alzheimer's disease. *Scientific Reports*, 5(1):9748, 2015.

William W Beatty, Nelson Butters, and David S Janowsky. Patterns of memory failure after scopolamine treatment: implications for cholinergic hypotheses of dementia. *Behavioral and Neural Biology*, 45(2):196–211, 1986.

John M Beggs. *The Cortex and the Critical Point: Understanding the Power of Emergence*. MIT Press, 2022.

John M Beggs and Dietmar Plenz. Neuronal avalanches in neocortical circuits. *Journal of Neuroscience*, 23(35): 11167–11177, 2003.

John M Beggs and Nicholas Timme. Being critical of criticality in the brain. *Frontiers in Physiology*, 3:163, 2012.

Timothy Bellay, Andreas Klaus, Saurav Seshadri, and Dietmar Plenz. Irregular spiking of pyramidal neurons organizes as scale-invariant neuronal avalanches in the awake state. *Elife*, 4:e07224, 2015.

Joydeep Bhattacharya, J Edwards, Adam N Mamelak, and Erin M Schuman. Long-range temporal correlations in the spontaneous spiking of neurons in the hippocampal-amygdala complex of humans. *Neuroscience*, 131(2):547–555, 2005.

Joschka Boedecker, Oliver Obst, Joseph T Lizier, N Michael Mayer, and Minoru Asada. Information processing in echo state networks at the edge of chaos. *Theory in Biosciences*, 131(3):205–213, 2012.

Paulo Henrique Botton, Marcelo S Costa, Ana Paula Ardais, Sabrina Mioranzza, Diogo O Souza, João Batista Teixeira da Rocha, and Lisiane O Porciúncula. Caffeine prevents disruption of memory consolidation in the inhibitory avoidance and novel object recognition tasks by scopolamine in adult mice. *Behavioural Brain Research*, 214(2): 254–259, 2010.

Elena Brazhnik, Ramie Borgnis, Robert U Muller, and Steven E Fox. The effects on place cells of local scopolamine dialysis are mimicked by a mixture of two specific muscarinic antagonists. *Journal of Neuroscience*, 24(42): 9313–9323, 2004.

ES Brazhnik, RU Muller, and SE Fox. Muscarinic blockade slows and degrades the location-specific firing of hippocampal pyramidal cells. *Journal of Neuroscience*, 23(2):611–621, 2003.

Denise J Cai, Daniel Aharoni, Tristan Shuman, Justin Shobe, Jeremy Biane, Weilin Song, Brandon Wei, Michael Veshkini, Mimi La-Vu, Jerry Lou, et al. A shared neural ensemble links distinct contextual memories encoded close in time. *Nature*, 534(7605):115–118, 2016.

Jiu Chen, Siyu Wang, Rong Chen, and Yong Liu. Neuroimaging biomarkers and cognition in Alzheimer's disease spectrum. *Frontiers in Aging Neuroscience*, 14, 2022.

Kelly B Clancy, Aaron C Koralek, Rui M Costa, Daniel E Feldman, and Jose M Carmena. Volitional modulation of optically recorded calcium signals during neuroprosthetic learning. *Nature Neuroscience*, 17(6):807–809, 2014.

Aaron Clauset, Cosma Rohilla Shalizi, and Mark EJ Newman. Power-law distributions in empirical data. *SIAM Review*, 51(4):661–703, 2009.

Wesley P Clawson, Nathaniel C Wright, Ralf Wessel, and Woodrow L Shew. Adaptation towards scale-free dynamics improves cortical stimulus discrimination at the cost of reduced detection. *PLoS Computational Biology*, 13(5): e1005574, 2017.

Luca Cocchi, Leonardo L Gollo, Andrew Zalesky, and Michael Breakspear. Criticality in the brain: A synthesis of neurobiology, models and cognition. *Progress in Neurobiology*, 158:132–152, 2017.

Samantha D Creighton, Heather A Collett, Paula M Zonneveld, Raiva A Pandit, Andrew E Huff, Kristen H Jardine, Bruce L McNaughton, and Boyer D Winters. Development of an "object category recognition" task for mice: Involvement of muscarinic acetylcholine receptors. *Behavioral Neuroscience*, 133(5):527, 2019.

David Dahmen, Sonja Grün, Markus Diesmann, and Moritz Helias. Second type of criticality in the brain uncovers rich multiple-neuron dynamics. *Proceedings of the National Academy of Sciences*, 116(26):13051–13060, 2019.

Gustavo Deco and Viktor K Jirsa. Ongoing cortical activity at rest: criticality, multistability, and ghost attractors. *Journal of Neuroscience*, 32(10):3366–3375, 2012.

Gustavo Deco, Viktor K Jirsa, and Anthony R McIntosh. Emerging concepts for the dynamical organization of resting-state activity in the brain. *Nature Reviews Neuroscience*, 12(1):43–56, 2011.

J C Dodart, C Mathis, and A Ungerer. Scopolamine-induced deficits in a two-trial object recognition task in mice. *Neuroreport*, 8(5):1173–1178, 1997.

Zhe Dong, William Mau, Yu Susie Feng, Zachary T Pennington, Lingxuan Chen, Yosif Zaki, Kanaka Rajan, Tristan Shuman, Daniel Aharoni, and Denise J Cai. Minian: An open-source miniscope analysis pipeline. *bioRxiv*, 2021.

Abdel Ennaceur. Object novelty recognition memory. In *Handbook of Behavioral Neuroscience*, volume 27, pages 1–22. Elsevier, 2018.

Erik D Fagerholm, Romy Lorenz, Gregory Scott, Martin Dinov, Peter J Hellyer, Nazanin Mirzaei, Clare Leeson, David W Carmichael, David J Sharp, Woodrow L Shew, et al. Cascades and cognitive state: focused attention incurs subcritical dynamics. *Journal of Neuroscience*, 35(11):4626–4634, 2015.

Erik D Fagerholm, Gregory Scott, Woodrow L Shew, Chenchen Song, Robert Leech, Thomas Knöpfel, and David J Sharp. Cortical entropy, mutual information and scale-free dynamics in waking mice. *Cerebral cortex*, 26(10): 3945–3952, 2016.

Erik D Fagerholm, W Matthew C Foulkes, Yasir Gallero-Salas, Fritjof Helmchen, Karl J Friston, Robert Leech, and Rosalyn J Moran. Neural systems under change of scale. *Frontiers in Computational Neuroscience*, 15:643148, 2021.

Leandro J Fosque, Rashid V Williams-García, John M Beggs, and Gerardo Ortiz. Evidence for quasicritical brain dynamics. *Physical Review Letters*, 126(9):098101, 2021.

Daniel Fraiman, Pablo Balenzuela, Jennifer Foss, and Dante R Chialvo. Ising-like dynamics in large-scale functional brain networks. *Physical Review E*, 79(6):061922, 2009.

Nir Friedman, Shinya Ito, Braden AW Brinkman, Masanori Shimono, RE Lee DeVille, Karin A Dahmen, John M Beggs, and Thomas C Butler. Universal critical dynamics in high resolution neuronal avalanche data. *Physical Review Letters*, 108(20):208102, 2012.

BH Gähwiler and DA Brown. Muscarine affects calcium-currents in rat hippocampal pyramidal cells in vitro. *Neuroscience Letters*, 76(3):301–306, 1987.

Stephane Gaskin, Marilyn Tardif, Emily Cole, Pavel Piterkin, Lima Kayello, and Dave G Mumby. Object familiarization and novel-object preference in rats. *Behavioural processes*, 83(1):61–71, 2010.

Shree Hari Gautam, Thanh T Hoang, Kylie McClanahan, Stephen K Grady, and Woodrow L Shew. Maximizing sensory dynamic range by tuning the cortical state to criticality. *PLoS Computational Biology*, 11(12):e1004576, 2015.

Kunal K Ghosh, Laurie D Burns, Eric D Cocker, Axel Nimmerjahn, Yaniv Ziv, Abbas El Gamal, and Mark J Schnitzer. Miniaturized integration of a fluorescence microscope. *Nature Methods*, 8(10):871–878, 2011.

Elakkat D. Gireesh and Dietmar Plenz. Neuronal avalanches organize as nested theta-and beta/gamma-oscillations during development of cortical layer 2/3. *Proceedings of the National Academy of Sciences*, 105(21):7576–7581, 2008.

Forough Habibollahi, Brett J Kagan, Daniela Duc, Anthony N Burkitt, and Chris French. Critical dynamics arise during structured information presentation: analysis of embodied in vitro neuronal networks. *bioRxiv*, 2022.

Gerald Hahn, Thomas Petermann, Martha N Havenith, Shan Yu, Wolf Singer, Dietmar Plenz, and Danko Nikolić. Neuronal avalanches in spontaneous activity in vivo. *Journal of Neurophysiology*, 104(6):3312–3322, 2010.

Gerald Hahn, Adrian Ponce-Alvarez, Cyril Monier, Giacomo Benvenuti, Arvind Kumar, Frédéric Chavane, Gustavo Deco, and Yves Frégnac. Spontaneous cortical activity is transiently poised close to criticality. *PLoS Computational Biology*, 13(5):e1005543, 2017.

Erika K Harding, Bruno Boivin, and Michael W Salter. Intracellular calcium responses encode action potential firing in spinal cord lamina i neurons. *Journal of Neuroscience*, 40(23):4439–4456, 2020.

Michael E Hasselmo. The role of acetylcholine in learning and memory. *Current Opinion in Neurobiology*, 16(6): 710–715, 2006.

Michael E Hasselmo and Bradley P Wyble. Free recall and recognition in a network model of the hippocampus: simulating effects of scopolamine on human memory function. *Behavioural Brain Research*, 89(1-2):1–34, 1997.

Peter Hayward. Acetylcholine and memory formation. *The Lancet Neurology*, 3(4):201, 2004.

Kristine Heiney, Vibeke Devold Valderhaug, Ioanna Sandvig, Axel Sandvig, Gunnar Tufte, Hugo Lewi Hammer, and Stefano Nichele. Evaluation of the criticality of in vitro neuronal networks: Toward an assessment of computational capacity. *arXiv preprint arXiv:1907.02351*, 2019.

Kari L. Hoffman and Bruce L. Mcnaughton. Coordinated reactivation of distributed memory traces in primate neocortex. *Science*, 297(5589):2070–2073, 2002.

EC Hulme, NJM Birdsall, ASV Burgen, and P Mehta. The binding of antagonists to brain muscarinic receptors. *Molecular Pharmacology*, 14(5):737–750, 1978.

Mostafa Jannesari, Alireza Saeedi, Marzieh Zare, Silvia Ortiz-Mantilla, Dietmar Plenz, and April A Benasich. Stability of neuronal avalanches and long-range temporal correlations during the first year of life in human infants. *Brain Structure and Function*, 225(3):1169–1183, 2020.

Manfred G Kitzbichler, Marie L Smith, Søren R Christensen, and Ed Bullmore. Broadband criticality of human brain network synchronization. *PLoS Computational Biology*, 5(3):e1000314, 2009.

Andreas Klaus, Shan Yu, and Dietmar Plenz. Statistical analyses support power law distributions found in neuronal avalanches. *PloS ONE*, 6(5):e19779, 2011.

Inge Klinkenberg and Arjan Blokland. The validity of scopolamine as a pharmacological model for cognitive impairment: A review of animal behavioral studies. *Neuroscience & Biobehavioral Reviews*, 34(8):1307–1350, 2010.

Timofey O Klyucherev, Pawel Olszewski, Alena A Shalimova, Vladimir N Chubarev, Vadim V Tarasov, Misty M Attwood, Stina Syvänen, and Helgi B Schiöth. Advances in the development of new biomarkers for Alzheimer's disease. *Translational Neurodegeneration*, 11(1):1–24, 2022.

Dylan Kotliar, Adrian Veres, M Aurel Nagy, Shervin Tabrizi, Eran Hodis, Douglas A Melton, and Pardis C Sabeti. Identifying gene expression programs of cell-type identity and cellular activity with single-cell rna-seq. *Elife*, 8: e43803, 2019.

Joanna Kowalczyk, Łukasz Kurach, Anna Boguszewska-Czubara, Krystyna Skalicka-Woźniak, Marta Kruk-Słomka, Jacek Kurzepa, Małgorzata Wydrzynska-Kuźma, Grażyna Biała, Adrianna Skiba, and Barbara Budzyńska. Bergapten improves scopolamine-induced memory impairment in mice via cholinergic and antioxidative mechanisms. *Frontiers in Neuroscience*, page 730, 2020.

Marta Kruk-Słomka, Agnieszka Michalak, Barbara Budzyńska, and Grażyna Biała. A comparison of mecamylamine and bupropion effects on memory-related responses induced by nicotine and scopolamine in the novel object recognition test in mice. *Pharmacological Reports*, 66(4):638–646, 2014.

JH Lee and EE El-Fakahany. Heterogeneity of binding of muscarinic receptor antagonists in rat brain homogenates. *Journal of Pharmacology and Experimental Therapeutics*, 233(3):707–714, 1985.

Marianne Leger, Anne Quiedeville, Valentine Bouet, Benoît Haelewyn, Michel Boulouard, Pascale Schumann-Bard, and Thomas Freret. Object recognition test in mice. *Nature Protocols*, 8(12):2531–2537, 2013.

Klaus Linkenkaer-Hansen, Vadim V Nikouline, J Matias Palva, and Risto J Ilmoniemi. Long-range temporal correlations and scaling behavior in human brain oscillations. *Journal of Neuroscience*, 21(4):1370–1377, 2001.

Fabrizio Lombardi, Oren Shriki, Hans J Herrmann, and Lucilla de Arcangelis. Long-range temporal correlations in the broadband resting state activity of the human brain revealed by neuronal avalanches. *Neurocomputing*, 461:657–666, 2021.

Zhengyu Ma, Gina G Turrigiano, Ralf Wessel, and Keith B Hengen. Cortical circuit dynamics are homeostatically tuned to criticality in vivo. *Neuron*, 104(4):655–664, 2019.

Najja Marshall, Nicholas M Timme, Nicholas Bennett, Monica Ripp, Edward Lautzenhiser, and John M Beggs. Analysis of power laws, shape collapses, and neural complexity: new techniques and matlab support via the ncc toolbox. *Frontiers in Physiology*, 7:250, 2016.

Stephanie R Miller, Shan Yu, and Dietmar Plenz. The scale-invariant, temporal profile of neuronal avalanches in relation to cortical γ–oscillations. *Scientific Reports*, 9(1):1–14, 2019.

Zoltán Nádasdy, Hajime Hirase, András Czurkó, Jozsef Csicsvari, and György Buzsáki. Replay and time compression of recurring spike sequences in the hippocampus. *Journal of Neuroscience*, 19(21):9497–9507, 1999.

Dylan M Nielson, Troy A Smith, Vishnu Sreekumar, Simon Dennis, and Per B Sederberg. Human hippocampus represents space and time during retrieval of real-world memories. *Proceedings of the National Academy of Sciences*, 112(35):11078–11083, 2015.

Hidetoshi Nishimori and Gerardo Ortiz. *Elements of phase transitions and critical phenomena*. Oup Oxford, 2010.

J Matias Palva, Alexander Zhigalov, Jonni Hirvonen, Onerva Korhonen, Klaus Linkenkaer-Hansen, and Satu Palva. Neuronal long-range temporal correlations and avalanche dynamics are correlated with behavioral scaling laws. *Proceedings of the National Academy of Sciences*, 110(9):3585–3590, 2013.

Thomas Petermann, Tara C Thiagarajan, Mikhail A Lebedev, Miguel AL Nicolelis, Dante R Chialvo, and Dietmar Plenz. Spontaneous cortical activity in awake monkeys composed of neuronal avalanches. *Proceedings of the National Academy of Sciences*, 106(37):15921–15926, 2009.

Matthew J Peterson, Sheena Geoghegan, and Larry W Lawhorne. An exploratory analysis of potential new biomarkers of cognitive function. *The Journals of Gerontology: Series A*, 74(3):299–305, 2019.

Eftychios A Pnevmatikakis, Daniel Soudry, Yuanjun Gao, Timothy A Machado, Josh Merel, David Pfau, Thomas Reardon, Yu Mu, Clay Lacefield, Weijian Yang, et al. Simultaneous denoising, deconvolution, and demixing of calcium imaging data. *Neuron*, 89(2):285–299, 2016.

Simon-Shlomo Poil, Richard Hardstone, Huibert D Mansvelder, and Klaus Linkenkaer-Hansen. Critical-state dynamics of avalanches and oscillations jointly emerge from balanced excitation/inhibition in neuronal networks. *Journal of Neuroscience*, 32(29):9817–9823, 2012.

Adrián Ponce-Alvarez, Adrien Jouary, Martin Privat, Gustavo Deco, and Germán Sumbre. Whole-brain neuronal activity displays crackling noise dynamics. *Neuron*, 100(6):1446–1459, 2018.

John M Power and Pankaj Sah. Nuclear calcium signaling evoked by cholinergic stimulation in hippocampal CA1 pyramidal neurons. *Journal of Neuroscience*, 22(9):3454–3462, 2002.

Viola Priesemann and Oren Shriki. Can a time varying external drive give rise to apparent criticality in neural systems? *PLoS Computational Biology*, 14(5):e1006081, 2018.

Viola Priesemann, Mario Valderrama, Michael Wibral, and Michel Le Van Quyen. Neuronal avalanches differ from wakefulness to deep sleep–evidence from intracranial depth recordings in humans. *PLoS Computational Biology*, 9 (3):e1002985, 2013.

Viola Priesemann, Michael Wibral, Mario Valderrama, Robert Pröpper, Michel Le Van Quyen, Theo Geisel, Jochen Triesch, Danko Nikolić, and Matthias HJ Munk. Spike avalanches in vivo suggest a driven, slightly subcritical brain state. *Frontiers in Systems Neuroscience*, 8:108, 2014.

Jiangbo Pu, Hui Gong, Xiangning Li, and Qingming Luo. Developing neuronal networks: self-organized criticality predicts the future. *Scientific Reports*, 3(1):1–6, 2013.

AM Raid, WM Khedr, MA El-Dosuky, and Mona Aoud. Image restoration based on morphological operations. *International Journal of Computer Science, Engineering and Information Technology (IJCSEIT)*, 4(3):9–21, 2014.

Tiago L Ribeiro, Mauro Copelli, Fábio Caixeta, Hindiael Belchior, Dante R Chialvo, Miguel AL Nicolelis, and Sidarta Ribeiro. Spike avalanches exhibit universal dynamics across the sleep-wake cycle. *PloS ONE*, 5(11):e14129, 2010.

Kim San Tang. The cellular and molecular processes associated with scopolamine-induced memory deficit: A model of Alzheimer's biomarkers. *Life Sciences*, 233:116695, 2019.

Silvia Scarpetta and Antonio de Candia. Neural avalanches at the critical point between replay and non-replay of spatiotemporal patterns. *PLoS ONE*, 8(6):e64162, 2013.

Abigail G Schindler, Shuang Li, and Charles Chavkin. Behavioral stress may increase the rewarding valence of cocaine-associated cues through a dynorphin/κ-opioid receptor-mediated mechanism without affecting associative learning or memory retrieval mechanisms. *Neuropsychopharmacology*, 35(9):1932–1942, 2010.

James P Sethna, Karin A Dahmen, and Christopher R Myers. Crackling noise. *Nature*, 410(6825):242–250, 2001.

Woodrow L Shew, Hongdian Yang, Shan Yu, Rajarshi Roy, and Dietmar Plenz. Information capacity and transmission are maximized in balanced cortical networks with neuronal avalanches. *Journal of Neuroscience*, 31(1):55–63, 2011.

Woodrow L Shew, Wesley P Clawson, Jeff Pobst, Yahya Karimipanah, Nathaniel C Wright, and Ralf Wessel. Adaptation to sensory input tunes visual cortex to criticality. *Nature Physics*, 11(8):659–663, 2015.

Jaana Simola, Alexander Zhigalov, Isabel Morales-Muñoz, J Matias Palva, and Satu Palva. Critical dynamics of endogenous fluctuations predict cognitive flexibility in the go/nogo task. *Scientific Reports*, 7(1):1–10, 2017.

Vladimir P Sotskov, Nikita A Pospelov, Viktor V Plusnin, and Konstantin V Anokhin. Calcium imaging reveals fast tuning dynamics of hippocampal place cells and CA1 population activity during free exploration task in mice. *International journal of molecular sciences*, 23(2):638, 2022.

F Paul Spitzner, Jonas Dehning, Jens Wilting, Annika Hagemann, J P. Neto, Johannes Zierenberg, and Viola Priesemann. Mr. estimator, a toolbox to determine intrinsic timescales from subsampled spiking activity. *PloS ONE*, 16(4): e0249447, 2021.

Vishnu Sreekumar, Simon Dennis, Isidoros Doxas, Yuwen Zhuang, and Mikhail Belkin. The geometry and dynamics of lifelogs: discovering the organizational principles of human experience. *PloS ONE*, 9(5):e97166, 2014.

Vishnu Sreekumar, Simon Dennis, and Isidoros Doxas. The episodic nature of experience: a dynamical systems analysis. *Cognitive science*, 41(5):1377–1393, 2017.

Craig V Stewart and Dietmar Plenz. Inverted-u profile of dopamine–nmda-mediated spontaneous avalanche recurrence in superficial layers of rat prefrontal cortex. *Journal of Neuroscience*, 26(31):8148–8159, 2006.

Carsen Stringer, Marius Pachitariu, Nicholas Steinmetz, Matteo Carandini, and Kenneth D Harris. High-dimensional geometry of population responses in visual cortex. *Nature*, 571(7765):361–365, 2019.

Dechuan Sun, Ranjith Rajasekharan Unnithan, and Chris French. Scopolamine impairs spatial information recorded with "miniscope" calcium imaging in hippocampal place cells. *Frontiers in Neuroscience*, 15:640350, 2021.

Enzo Tagliazucchi, Pablo Balenzuela, Daniel Fraiman, and Dante R Chialvo. Criticality in large-scale brain fmri dynamics unveiled by a novel point process analysis. *Frontiers in Physiology*, 3:15, 2012.

Christian Tetzlaff, Samora Okujeni, Ulrich Egert, Florentin Wörgötter, and Markus Butz. Self-organized criticality in developing neuronal networks. *PLoS Computational Biology*, 6(12):e1001013, 2010.

Chris J Tinsley, Nadine S Fontaine-Palmer, Maria Vincent, Emma PE Endean, John P Aggleton, Malcolm W Brown, and E Clea Warburton. Differing time dependencies of object recognition memory impairments produced by nicotinic and muscarinic cholinergic antagonism in perirhinal cortex. *Learning & Memory*, 18(7):484–492, 2011.

Daniel Toker, Ioannis Pappas, Janna D Lendner, Joel Frohlich, Diego M Mateos, Suresh Muthukumaraswamy, Robin Carhart-Harris, Michelle Paff, Paul M Vespa, Martin M Monti, et al. Consciousness is supported by near-critical slow cortical electrodynamics. *Proceedings of the National Academy of Sciences*, 119(7):e2024455119, 2022.

Jonathan Touboul and Alain Destexhe. Can power-law scaling and neuronal avalanches arise from stochastic dynamics? *PloS ONE*, 5(2):e8982, 2010.

Jonathan Touboul and Alain Destexhe. Power-law statistics and universal scaling in the absence of criticality. *Physical Review E*, 95(1):012413, 2017.

Eric M Trautmann, Daniel J O'Shea, Xulu Sun, James H Marshel, Ailey Crow, Brian Hsueh, Sam Vesuna, Lucas Cofer, Gergő Bohner, Will Allen, et al. Dendritic calcium signals in rhesus macaque motor cortex drive an optical brain-computer interface. *Nature Communications*, 12(1):3689, 2021.

Hiroshi Tsubokawa and William N Ross. Muscarinic modulation of spike backpropagation in the apical dendrites of hippocampal CA1 pyramidal neurons. *Journal of Neuroscience*, 17(15):5782–5791, 1997.

Gerhard Werner. Consciousness viewed in the framework of brain phase space dynamics, criticality, and the renormalization group. *Chaos, Solitons & Fractals*, 55:3–12, 2013.

Meredith Wicklund and Ronald C Petersen. Emerging biomarkers in cognition. *Clinics in geriatric medicine*, 29(4): 809–828, 2013.

Rashid V Williams-García, Mark Moore, John M Beggs, and Gerardo Ortiz. Quasicritical brain dynamics on a nonequilibrium widom line. *Physical Review E*, 90(6):062714, 2014.

Jens Wilting and Viola Priesemann. Inferring collective dynamical states from widely unobserved systems. *Nature Communications*, 9(1):1–7, 2018.

Jens Wilting and Viola Priesemann. Between perfectly critical and fully irregular: A reverberating model captures and predicts cortical spike propagation. *Cerebral Cortex*, 29(6):2759–2770, 2019.

Hannah S Wirtshafter and John F Disterhoft. In vivo multi-day calcium imaging of CA1 hippocampus in freely moving rats reveals a high preponderance of place cells with consistent place fields. *Journal of Neuroscience*, 42(22): 4538–4554, 2022.

Julia M Yeomans. *Statistical mechanics of phase transitions*. Clarendon Press, 1992.

Pengcheng Zhou, Shanna L Resendez, Jose Rodriguez-Romaguera, Jessica C Jimenez, Shay Q Neufeld, Andrea Giovannucci, Johannes Friedrich, Eftychios A Pnevmatikakis, Garret D Stuber, Rene Hen, et al. Efficient and accurate extraction of in vivo calcium signals from microendoscopic video data. *Elife*, 7:e28728, 2018.

Vincent Zimmern. Why brain criticality is clinically relevant: A scoping review. *Frontiers in Neural Circuits*, 14:54, 2020.

A Supplementary Materials

A.1 Ethical Considerations

All surgical and experimental procedures were approved by the Florey Animal Ethics Committee (No. 20-060UM) and were conducted in strict accordance with the Australian Animal Welfare Committee guidelines.

A.2 Subjects

Eight naive adult male C57BL/6 mice aged 6 weeks were housed in The Florey Institute of Neuroscience and Mental Health, Melbourne. All animals weighed 27–30 g (28.5 g $\pm$ 0.679 g) at the time of surgery and were housed individually. The facility was kept on a 12-12 hour light-dark schedule, with the lights on from 7:30 am to 7:30 pm. The mice had *ad libitum* access to standard chow and water.

A.3 Stereotaxic Surgery

We aimed to use miniaturized fluorescence microscopes, or miniscopes, as our means for *in vivo* calcium imaging from large populations of neurons in awake and behaving animals. The surgical procedures for this technique comprised two components: viral infusion and GRadient INdex (GRIN) lens implantation.

A.3.1 Virus Infusion

A custom made injection system was used to inject the pAAV.Syn.GCaMP6f.WPRE.SV40 virus (500 nL, viral load: 2.2 $\times$ $10^1$3 GC/ml; AddGene, United States) into the dorsal hippocampus (AP -2.1, ML +2.1, DV -1.7 relative to bregma) over a duration of 15 minutes. The virus was initially loaded into a capillary (with an interior diameter of 0.9 mm) created using a Sutter P-1000 electrode puller to produce a tip diameter of 20-50 μm. The open end was then sealed using silicon oil (Sigma-Aldrich, United States); The virus volume was controled by a round brass rod (diameter: 0.8 mm; Albion Alloys, United Kingdom), connected to 3D positioner which was fitted into the capillary. Following viral injection, the virus injector remained in place for an additional 10 minutes to allow for viral diffusion. The animal was then left to recover for one week to enable fluorophore expression.

A.3.2 GRIN Lens Implantation

Anchors were implanted by placing two 1 mm screws at coordinates AP +1.8, ML -2.5 and AP -2.8, ML -0.8. A small section of the skull, centered at AP -2.1, ML +1.6, was removed using a 2 mm drill bur, and the exposed dura was carefully cleaned using fine tweezers. AA 27-gauge blunt needle was used to aspirate the cortex, exposing the vertical striations of the hippocampal fimbria. Artificial cerebrospinal fluid was flowed during the procedure to keep the operating field clear. The GRIN lens (0.25 pitch, #64-519, Edmund Optics) was implanted 1.35 mm deep into the tissue surface, with the most posterior point of the drilled hole (next to lambda side) serving as a reference point (Cai et al., 2016). To prevent movement of the implanted GRIN lens, cyanoacrylate glue was applied around the lens

and dental cement was applied for additional support. The lens was further protected by applying fast-setting silicone adhesive (Dragon Skin Series ®, United States). Following the surgery, the animal received intraperitoneal injections of Meloxicam (2 mg/kg) daily to alleviate pain and inflammation. Additionally, enrofloxacin water (1:150 dilution, Baytril ®, United States) was provided to the animal for one week. Four weeks after the initial surgery, a metal baseplate was attached to the animal's head to hold the miniscope in place at the optimal focal distance. It should be noted that this step is not considered a surgical procedure.

A.4 Training

Following the surgery, the animals were handled twice a day for approximately 10 minutes during the daytime, and their weight was measured after each handling session for five days. For 3 days prior to recordings, the animals were habituated to wearing the miniscope and moving around freely with the device attached to their heads for 10 minutes per day.

A.5 Experimental Procedures and Behavioural Tasks

All the recordings were performed during the daytime. The animal was brought into a silent recording room 30 min before the start of recording to acclimate to the surrounding environment.

The standard novel object recognition (NOR) test was performed using the protocols introduced in previous works (Ennaceur, 2018; Leger et al., 2013). This task was conducted in a square-shaped plastic open field arena of size 33 cm $\times$ 33 cm $\times$ 20 cm. Two identical objects of exact same color and shape were chosen for the familiarization phase. A third (novel) object consistent in height and volume but different in shape, color, and appearance was used for the testing phase. All objects were odorless, brightly colored, not chewable, and of a shape and weight which did not allow mice to climb over them or knock them over.

During habituation, the animals were allowed to explore the empty arena for 10 minutes per day and 3 days prior to the experiment day. Twenty-four hours after the last session of habituation, the NOR experiments started where animals were exposed to the familiar arena with the two identical objects placed diagonally inside the arena and at an equal distance from the walls for a 15-minute recording session (familiarization phase). After a 10-minute inter-session-interval inside the animal's home cage, the mice were allowed to explore the open field for another 15 minutes in the presence of one familiar object and the novel object to test long-term recognition memory (testing phase). The arena was cleaned with 80% ethanol to eliminate scent clues before the first day of habituation and was kept intact during the remainder of the experiment. All the objects were also cleaned with 80% ethanol before each recording session.

On the experiment day, prior to the familiarization phase, a 15-minute recording session was performed inside the animal's home cage as the baseline control. Custom-made miniscope acquisition software was used to record imaging frames during all the recording sessions at a sampling rate of 30 FPS. The miniscope cable was suspended over the open arena through a custom-made commutator. TopScan (TopView Analyzing System 2.0; Clever Sys Inc.), as a

top-view-based behavior analysis system, was used to detect and follow animal body parts and provide accurate behavior analysis results during NOR familiarization and testing phases.

A.5.1 Scopolamine injection

One month after the completion of NOR experiments on the healthy animals, 2 were removed from the study due to showing signs of reduced mobility and a significant increase in the level of their struggle while mounting miniscope devices on their baseplates. The remaining 6 animals were employed in another set of repeated NOR experiments (all settings and protocols identical to those above). In the first week, the animals were injected with a dose of saline (0.9% NaCl, intraperitoneal, i.p.; 10 mL/kg body mass), 20 minutes before the familiarization phase of NOR (Tinsley et al., 2011). After 2 weeks of no experiments, the same 6 animals were injected with a dose of scopolamine (intraperitoneal, i.p.; 0.6 mg/kg body mass) 20 minutes before the familiarization phase of NOR. Scopolamine hydrobromide (Sigma-Aldrich, United States) was dissolved in sterile 0.9% saline. This was followed by the regular protocols for both phases of NOR while recording the same CA1 neuronal networks using Miniscopes.

A.6 Data processing

The acquired data from an experimental session with any given length consist of sequential recording files each including 100 frames. The frames were all captured from the GIRN lens field of view with a frequency of 30 Hz and each frame has a size of 480×752 pixels.

To start with the processing pipeline, inspired by previous work and utilizing the minian package (Dong et al., 2021) [2], we introduce *Pre-Processing*, *Background Removal*, *Motion Correction*, *Initialization of Constrained Non-negative Matrix Factorization (CNMF)*, and *CNMF* as the prominent building blocks of our workflow.

A.6.1 Pre-processing

For cases where the active neuronal population did not expand the entire field of view, the region of interest was a subset in all the video frames. Next, a glow removal step was carried out by calculating a minimum projection across all frames and subtracting it from all. When the glow in the background was removed, the recordings were denoised frame by frame. Denoising was done using a median filter on each frame with a kernel size that must be chosen according to the size of the largest cells in the field of view. Usually, an effective kernel size is assumed to equal half the diameter of the largest cell present in the video file (Dong et al., 2021).

A.6.2 Background removal

In this step, the background in each frame (everything except the fluorescent signal of in-focus cells) was estimated and removed. For this cause, Morphological Erosion and Dilation (Raid et al., 2014) were used respectively with the window size equal to the expected size of the largest cell diameter. This was also done frame by frame. In the erosion

[2] https://github.com/DeniseCaiLab/minian

process, each pixel was replaced by the minimum value within the filter window, and hence any bright features that appeared smaller than the window diameter were converted to zero brightness. Following this conversion, the dilation operation, to replace each pixel with the maximum value in the filter window, is basically the reverse procedure to bring back all the bright features except those completely eliminated. The morphological opening method obtains a good estimation of the background by removing the bright cells if the window size matches the expected cell diameter. This estimated background was then removed from all cells.

A.6.3 Motion correction

At this step, firstly, the frame with maximum projection values was selected as the base frame. Then, for all other frames, a two-dimensional cross-correlation between that frame and the base frame was calculated using a fast Fourier transform (fft). Next, the frame with the maximum correlation was chosen and its inverse value was applied as the required correction shift to all frames.

A.6.4 Initialization of CNMF

To utilize the Constrained Non-negative Matrix Factorization (CNMF) algorithm (Zhou et al., 2018; Pnevmatikakis et al., 2016; Kotliar et al., 2019) on our data, an initial estimation of the spatial footprints and temporal activity traces of the neural population was required. This was done using the seed selection procedure and refinement of initial seeds by signal-to-noise ratio (SNR) evaluation in the minian pipeline (Dong et al., 2021) and initializing the spatial footprint and temporal activity matrices.

A.6.5 CNMF

Finally, the CNMF technique to extract an accurate estimation of the spatial footprints and temporal activities of the cells, as well as the same information about the background, was performed (Zhou et al., 2018; Pnevmatikakis et al., 2016). This method employs a constrained deconvolution (CD) approach to seek the sparsest activity signal which defines the observed fluorescence intensities up to an estimated measurement noise level.

A.7 Data analysis

We binarized the Calcium signals of each neuron in each recorded frame (i.e., 33.3 ms) based on being active or not, i.e., 1 and 0. The *network activity* as the sum of all recorded activity within the same time frame was then calculated. *neuronal avalanches* were then defined based on the network activity by applying a threshold at the 60th percentile of total network activity (Poil et al., 2012). Consistent with critical systems, our results were robust across a range of thresholds (30 to 70%).

To demonstrate the criticality of a system, we investigated the presence of the following criteria in the dynamics of our data. These criteria are all necessary conditions of a critical regimen and together can show with a high confidence

whether the system lies near a critical point (Beggs and Plenz, 2003; Wilting and Priesemann, 2018).

A.8 Multiple power-laws

A critical system has units of information that show some fluctuation in their activity while maintaining a level of correlation among them. This implies that such a system is defined by scale-free dynamics and events in both spatial and temporal domains obey power-laws. Thus, events are contiguous cascades of neuronal activity rather than being limited to local bursts or huge firing of neurons consuming the network. These activities are called *neural avalanches*. If a system is performing near-criticality, we are looking for not just one but multiple power-law distributions fitted to various aspects of the system dynamics in different domains (Beggs and Timme, 2012; Yeomans, 1992; Nishimori and Ortiz, 2010).

To investigate this property in our system, we utilize the *neuronal avalanches*. We define the start and end points of an avalanche when the network activity crosses a threshold value (as stated above) from below and then above (Poil et al., 2012). The size of an avalanche, S, is the total number of events during the avalanche. The avalanche duration, D, is the time between threshold crossings. Similar to (Ma et al., 2019), we use maximum likelihood estimation to fit a truncated power-law to the avalanche size distribution:

$$f(S) = \frac{S^{-\tau}}{\sum_{S_{\min}}^{S_{\max}} S^{-\tau}} \tag{A.1}$$

where τ would be the power-law exponent corresponding to avalanche sizes. Assuming we have detected N_A avalanches in the recording files, the fitting process to obtain the above equation is an iterative procedure (Klaus et al., 2011):

1. Find the maximum avalanche size $S_{\max}$.
2. Evaluate the three different power-law exponents, τ, for 3 values of minimum avalanche sizes observed, $S_{\min}$.
3. Calculate the *Kolmogorov-Smirnov* or KS test for this estimation to determine the goodness-of-fit between the fitted power-law and empirical distribution.
4. Among the obtained KS values, choose the smallest one alongside the corresponding τ and $S_{\min}$ values.
5. Complete the estimation if KS $< \frac{1}{\sqrt{N_A}}$ or otherwise repeat steps 2 to 5 with $S_{\max}$ reduced by 1 until this condition is met.

Steps 3 to 5 are necessary to ensure the data distribution indeed comes from a power-law rather than another candid heavy-tailed distribution such as log normal and stretched exponential forms (Clauset et al., 2009).

Eventually, by applying the exact same procedure to the set of D values, the corresponding power-law exponent of α is calculated for avalanche duration distribution.

As proposed in (Ma et al., 2019), hypothesis testing was conducted to determine if a power law fit of an avalanche distribution was plausible. To achieve this, 1000 artificial power law distributions were generated using the same power

law exponent, the number of detected avalanches, and minimum and maximum avalanche sizes as the experimental distribution. These surrogate distributions were simulated using the inverse method as $S = S_{\min}(1-r)^{\frac{-1}{\tau-1}}$ where r is a random number sampled from a uniform distribution between 0 and 1. Based on the empirical data, we upper-truncated any surrogate distribution at the maximum cutoff equivalent to $S_{\max}$. After generating the simulated surrogate distributions, the KS statistics were employed to quantify how far they are from a perfect power law. A p value was thus determined as the ratio of the surrogate distributions with KS values smaller than those of the corresponding experimental avalanche distributions. We set the significance level to 0.05; meaning $p < 0.05$ implies a rejection of the power law hypothesis while $p \geq 0.05$ suggests the power law hypothesis was not rejected (the fit was good).

A.9 Exponent relation and Deviation from Criticality Coefficient (DCC)

In critical systems, there is another exponent relationship between the power law parameters (α and τ) and the exponent of mean avalanche sizes ($\langle S \rangle$), given their duration, D (Friedman et al., 2012). We first find this third power law exponent of the system, β, from the experimental data using linear regression given the following exponent relation is present in a critical system:

$$\langle S \rangle \propto D^{\beta_{\text{fit}}}. \tag{A.2}$$

This third power law exponent also relates the size and duration distributions of the avalanches and is predicted by:

$$\beta_{\text{pred}} = \frac{(\alpha - 1)}{(\tau - 1)}. \tag{A.3}$$

Comparing the fitted value from the empirical data (β_{fit}) and its estimation using α and τ exponents (β_{pred}), a new measure is derived to evaluate the *Deviation from Criticality Coefficient* (DCC), parameterised as d_{CC}:

$$d_{\text{CC}} = |\beta_{\text{pred}} - \beta_{\text{fit}}|, \tag{A.4}$$

where β_{pred} and β_{fit} are the predicted and fitted values of β respectively. Consequently, a smaller DCC value indicates a more accurately fit power law distribution to the empirical data.

A.10 Scaling function

According to (Friedman et al., 2012), the obtained β can be used to accomplish a scaling function for the avalanche shapes. In a critical system, all avalanche profiles of different sizes are scaled versions of the same shape.
For any given avalanche duration D, the average number of neurons firing at time t (within D seconds) is defined by $s(t, D)$. The following relations hold in this system:

$$s(t, D) \propto D^{\gamma} F\left(\frac{t}{D}\right)$$
$$\langle S \rangle(D) = \int_0^D s(t, D) dt \tag{A.5}$$

where $F(\frac{t}{D})$ is a universal function for all avalanches and is proportional to $\frac{t}{D}$ and $\gamma = \beta - 1$. Hence in this process, we use an initial β to predict γ and using this γ and the first term in Equation A.5, we get $F(\frac{t}{D})$ as $\langle \frac{s(t,D)}{D^{\gamma}} \rangle$. Here $\langle . \rangle$ denotes the average over all avalanches with duration D. A collection of $F(\frac{t}{D})$ functions are extracted for various D durations. The error for shape collapse is described as below:

$$\frac{\mathrm{var}(F)}{[\mathbf{max}(F) - \min(F)]^2} \tag{A.6}$$

Repeating this process with various values for β, we select the exponent which produces the smallest shape collapse error in Equation A.6 as the final scaling factor. In theory, we expect to obtain similar (if not the same) β values from this analysis and our estimations in Section A.9. We utilize the NCC toolbox in MATLAB (Marshall et al., 2016) to perform shape collapse on data. This shape collapse error is minimized under critical conditions. We used avalanches with durations between 4 and 20 bins (133.2 to 666 ms) for the shape collapse analysis. The avalanches recorded over the time course of the study were not abundant enough to conduct meaningful shape collapses beyond these cutoff points.

A.11 Branching ratio

The branching ratio is defined as the ratio of the number of neurons active at time $t + 1$ to the number of active neurons at time t. Since a critical regime is naturally balanced and avoids runaway gains, the branching ratio is supposed to be 1. Meaning on average, network activity neither saturates nor damps in time.

Let's assume we have detected N active neurons in total and the number of active neurons in each time step t is defined by $N(t)$. Considering a fixed branching ratio of m, we get $\langle N(t+1)|N(t) \rangle = mN(t) + h$ where $\langle | \rangle$ is the conditional expectation and h is modeling the mean rate of the external drive. The activity is stationary if $m < 1$, while it grows exponentially if $m > 1$ meaning that $m = 1$ separates these two regimens and represents a critical dynamic point. A precise prediction of m helps to a great extent while assessing the risk that $N(t)$ develops a large and devastating avalanche of events such as epileptic seizures.

Under the circumstances when the full activity $N(t)$ is known, m can be conventionally estimated using linear regression. However, under subsampling when we are aware only a fraction of neurons in a brain area is sampled, this conventional method will be biased by a certain amount. The bias vanishes only if all units are sampled because it is inherent to subsampling and cannot be overcome by obtaining longer recordings . Thus, we will instead work with the subsampled activity $n(t)$ where the fraction of recorded units to all cells is defined as a constant μ. $n(t)$ will be a random variable whose expectation is proportional to the real $N(t)$ and we have $< n(t)|N(t) >= \mu N(t) + \xi$ where μ and ξ are

constants. According to (Wilting and Priesemann, 2018), the bias value for the conventional linear estimator can now be calculated as:

$$\frac{m\mu^2 \mathrm{var}(N(t))}{\mathrm{var}(n(t)) - 1} \tag{A.7}$$

To overcome this subsampling bias, the method introduced by Wilting and Priesemann (2018) (Wilting and Priesemann, 2018) is utilized. Instead of directly using the biased regression of activity at time t and $t+1$, multiple linear regressions of activity between times t and $t+k$ are performed with different time lags $k = 1, \ldots, k_{\max} = 2000$. Each of these k values returns a regression coefficient r_k with r_1 being equal to the result of a conventional estimator of m. Under subsampling, all these regression slopes are biased by the same factor $b = \frac{\mu^2 \mathrm{var}(N(t))}{\mathrm{var}(n(t))}$. In these circumstances, instead of the exponential relation $r_k = m^k$ which is expected under full sampling, we should generalize this equation to:

$$r_k = \frac{\mu^2 \mathrm{var}(N(t))}{\mathrm{var}(n(t))}.m^k = b.m^k \tag{A.8}$$

Having multiple calculated r_k values, we can estimate both b and m which are constant for all k.

The above multiple-regression (MR) estimator is equivalent with estimating the autocorrelation time of sub-critical periodic autoregressive models (PARs), with equal autocorrelation and regression coefficients (r_k). While subsampling decreases the autocorrelation strength (r_k), the decay time of the autocorrelation is indeed preserved. This intrinsic timescale allows inferring the corresponding branching parameter m of the system. To estimate this intrinsic timescale, utilizing the toolbox introduced in (Spitzner et al., 2021), we used 1) an exponential function, as well as 2) a complex function featuring an oscillatory term, a Gaussian decay term, and an offset term as decay functions fitted to r_k values and reported the results from the chosen function with the highest goodness of fit.